Title

Frontal Bone Healing Is Sensitive to Wnt Signaling Inhibition via Lentiviral-Encoded Beta-Catenin Short Hairpin RNA.

Journal

Tissue engineering. Part A, 24(23-24)

ISSN

1937-3341

Authors

Zhang, Lei
Chang, Leslie
Xu, Jiajia
et al.

Publication Date

2018-08-01

DOI

10.1089/ten.tea.2017.0465

Peer reviewed

TISSUE ENGINEERING: Part A
Volume 24, Numbers 23 and 24, 2018

DOI: 10.1089/ten.tea.2017.0465

termis
Tissue Engineering
& Regenerative Medicine
International Society

ORIGINAL ARTICLE

Frontal Bone Healing Is Sensitive to Wnt Signaling Inhibition via Lentiviral-Encoded *Beta-Catenin* Short Hairpin RNA

Lei Zhang, MD,[1,2,*] Leslie Chang, BS,[1,3,*] Jiajia Xu, PhD,[1] Carolyn Ann Meyers, BS,[1] Noah Yan,[1] Erin Zou,[1] Catherine Ding,[4] Kang Ting, DMD, DMedSci,[4,5] Chia Soo, MD,[4,6] Shen Pang, PhD,[4] and Aaron W. James, MD, PhD[1,4]

The Wnt/β-catenin signaling pathway plays an integral role in skeletal biology, spanning from embryonic skeletal patterning through bone maintenance and bone repair. Most experimental methods to antagonize Wnt signaling *in vivo* are either systemic or transient, including genetic approaches, use of small-molecule inhibitors, or neutralizing antibodies. We sought to develop a novel, localized model of prolonged Wnt/β-catenin signaling blockade by the application and validation of a lentivirus encoding *β-catenin* short hairpin RNA (shRNA). Efficacy of lentiviral-encoded *β-catenin* shRNA was first confirmed *in vitro* using bone marrow mesenchymal stromal cells, and *in vivo* using an intramedullary long bone injection model in NOD SCID mice. Next, the effects of *β-catenin* knockdown were assessed in a calvarial bone defect model, in which the frontal bone demonstrates enhanced bone healing associated with heightened Wnt/β-catenin signaling. Lentivirus encoding either *β-catenin* shRNA or random sequence shRNA with enhanced green fluorescent protein (control) was injected overlying the calvaria of NOD SCID mice and bone defects were created in either the frontal or parietal bones. Among mice treated with lentivirus encoding *β-catenin* shRNA, frontal bone defect healing was significantly reduced by all radiographic and histologic metrics. In contrast, parietal bone healing was minimally impacted by *β-catenin* shRNA. In aggregate, our data document the application and validation of a lentivirus encoding *β-catenin* shRNA model that represents an easily replicable tool for examining the importance of locoregional Wnt/β-catenin signaling in bone biology and regeneration.

Keywords: Wnt signaling, bone healing, bone repair, osteogenesis, skull, calvaria, *beta-catenin* shRNA, calvarial bone defect, intramembranous bone, membranous bone

Introduction

The Wnt signaling pathway plays a widespread role in both development and disease, including directing cell proliferation, polarity, and cell fate decisions. Broadly, Wnt signaling can be divided into noncanonical and canonical pathways. Canonical Wnt signaling regulates β-catenin protein accumulation in the cytoplasm and transcriptional activation of target genes that regulate skeletogenesis (see MacDonald *et al.*[1] for a review of the Wnt signaling pathway). The Wnt/β-catenin pathway spans embryonic skeletal patterning through fetal skeletal development and is key mediator of bone modeling and remodeling.[2] This pathway regulates cellular differentiation in bone precursors, including osteoblasts.[3] Better understanding of the regulatory mechanism and effect of pathophysiological Wnt signaling is important in the development of novel therapies in regenerative medicine.

As the Wnt family is an important mediator of bone formation, we sought to develop a localized, temporally controlled method to disrupt canonical Wnt signaling. This model would allow us to characterize the importance of Wnt signaling in endogenous bone repair, as well as better examine local osteoinductive factors that potentiate Wnt/β-catenin signaling in combination with other osteoblastogenic

[1]Department of Pathology, Johns Hopkins University, Baltimore, Maryland.
[2]Department of Oral and Maxillofacial Surgery, School of Stomatology, China Medical University, Shenyang, China.
[3]University of California San Diego School of Medicine, La Jolla, California.
[4]UCLA and Orthopaedic Hospital Department of Orthopaedic Surgery and the Orthopaedic Hospital Research Center, Los Angeles, California.
[5]Division of Growth and Development and Section of Orthodontics, School of Dentistry, UCLA, Los Angeles, California.
[6]Division of Plastic and Reconstructive Surgery, Department of Surgery, David Geffen School of Medicine, University of California, Los Angeles, California.
*These two authors have equal contribution.

signaling pathways.[4] Currently available experimental models to disrupt Wnt signaling *in vivo* in a locoregional manner all have drawbacks. Small-molecule inhibitors[5] have potential off-target effects, while neutralizing antibodies[6] have concerns with tissue bioavailability and prolonged bioactivity. Few of these molecules have demonstrated selectivity studies, limiting our understanding of the systemic effects particularly as each structure may have subtle differences in interactions with β-catenin/Tcf, β-catenin/E-cadherin, and β-catenin/adenomatous polyposis coli (APC) complexes. Transgenic mouse model[7,8] has also been used to knock out β-catenin. Although localized β-catenin knockout is possible using tamoxifen inducible Cre recombinase Ctnnb1 mice, PCR analysis demonstrates residual β-catenin from KO animals making this an incomplete knockout.[9]

Therefore, we aimed to design an efficient model for localized and temporally controlled Wnt/β-catenin signaling inhibition in osseous tissues. RNA interference is a powerful technique that can be used to study gene function in mammalian cells. There are multiple mechanisms to delete gene function, such as the use of short interfering RNA (siRNA), which inactivates target gene expression before translation into protein. siRNA gene knockdown has been previously utilized in the Wnt/β-catenin pathway to understand effects on neoplastic tissue and cell lines.[10–12] However, increasing concern with the probability of off-target effects,[13] as well as nondurable long-term gene silencing,[14] makes use of siRNA in *in vivo* models limited. Short hairpin RNA (shRNA) infection with viral vectors generates stable knockdown due to integration into DNA, reducing the need for multiple rounds of transfection and greater reproducibility. Although there are multiple methods of shRNA delivery, viruses are the most efficient vectors as they are a proficient intracellular gene delivery method with nuclear localization.[15] Among the viruses, lentiviral vectors are an attractive option as they provide stable vector integration into the host genome and infection of both mitogenic and quiescent cells.[16] In addition, they are generally less toxic for cells than adenoviral-mediated transduction.[17] Finally, local delivery of shRNA accesses the target cell population directly, allowing for locoregional knockdown of the targeted gene.

In this study, we report on the application and validation of a lentivirus encoding *β-catenin* shRNA structure. In sequential studies, we first validated the vector using bone marrow mesenchymal stromal cells (BMSCs) *in vitro*, followed by exposure of the *in vivo* bone marrow milieu via percutaneous intramarrow injection of the *β-catenin* shRNA lentivirus. Finally, we validated our findings using a model of membranous bone defect healing. In this study, frontal and parietal bone defects were created in mice pretreated with lentiviral-delivered *β-catenin* shRNA. Prior investigators have shown that the frontal bone, a neural crest-derived bone, demonstrates enhanced bone healing along with increased Wnt/β-catenin pathway activation.[18] We hypothesized that frontal bone healing would show sensitivity to our model of canonical Wnt signaling inhibition.

Materials and Methods

Antibodies and reagents

The following primary antibodies were used: anti-green fluorescent protein (GFP, A-21311; 1:200; Thermo Fisher Scientific), anti-Axin2 (ab32197, 1:200; Abcam Biotechnology), and antiproliferating cell nuclear antigen (PCNA, ab18897, 1:200; Abcam). Secondary antibody: DyLight 594 (DI-1594, 1:200; Vector Laboratories) (see Supplementary Table S1; Supplementary Data are available online at www.liebertpub.com/tea).

Viral production and purification

The lentiviral vector encoding *β-catenin* lentivirus shRNA or enhanced GFP (eGFP) with random sequence shRNA (control shRNA) was generated by cotransfection of 293T cells with the *β-catenin* shRNA plasmid pLKO.1 (10878; Addgene) (see Supplementary Fig. S1 for the structure map), and the helper plasmids pCMV-dR8.2-vprX and pCMB.VSVG. β-Catenin targeting sequence is GCTTGGAATGAGACTGCTGAT. Control shRNAs were targeted against GFP. Following transduction, cells were selected with puromycin. The viral vector was collected from transfected cell cultures, and cell debris was removed through 0.22 mm filtration and concentrated by Ultrafuge at 4°C, 17,000 rpm for 60 min using Beckman SW32 rotors. The pellets that contained the lentiviral vector were resuspended with Dulbecco's modified Eagle's medium (DMEM) to bring the concentration from 7.8×10^6 to 5×10^7 tissue culture infective dosage ($TCID_{50}$)/mL for *β-catenin* shRNA or control shRNA. Lentiviral vector titer was estimated by measuring the gag p24 protein, 1 pg of p24 reading was assigned as 10 $TCID_{50}$ for freshly isolated lentiviral vectors.

Human BMSC isolation

Human BMSCs were obtained from deidentified hip arthroplasty specimens in otherwise well individuals with adaptation from previous reports.[4] Cells were seeded onto six-well plates at a density of 1×10^5 cells per well in DMEM (Gibco) containing 10% fetal bovine serum (Thermo Fisher Scientific, Inc.), 100 U/mL of penicillin, and 100 mg/mL of streptomycin (Gibco). Cultures were kept at 37°C in a humidified atmosphere containing 95% air and 5% CO_2. For all assays, cells from passage 2 only were used for experiments. Human BMSCs were treated with lentivirus encoding *β-catenin* shRNA and control shRNA lentivirus ($n=3$ for each group). Three days later, quantitative real time-polymerase chain reaction (qRT-PCR) was used to analyze the *β-catenin* expression in *β-catenin* shRNA or control shRNA-transfected BMSCs.

Animals

All animal experiments were performed according to the approved protocol of the Animal Care and Use Committee at UCLA or Johns Hopkins University, purchased from Jackson Laboratory. For intramedullary injection model, 8-week-old male NOD SCID mice were used (NOD.CB17-Prkdc^{scid}/J), while for the calvarial defect model, 19-week-old male NOD SCID mice were used (see Supplementary Table S2 for animal allocation). Each was housed in a single pathogen-free ventilated cage, fed a standard rodent chow diet, and provided tap water *ad libitum*. All anesthesia was performed with 2–3% isoflurane in 100% oxygen at a flow

rate of 1 L/min and operated upon on a warm, small animal surgery station.

Intramarrow lentiviral injection

Intramarrow lentiviral injection was performed, adapted from our previously reported methods.[19] The right knee was sterilized with Betadine Scrub®. A 5 mm-longitudinal incision was made along the medial aspect of the quadriceps-patellar complex. The patella was dislocated laterally to expose the intercondylar groove. A 0.9 mm k-wire on a trephine drill was used to create a trephination defect. Using a 1-mL syringe with 27-gauge needle, *β-catenin* shRNA or eGFP-shRNA control (5×10^7 $TCID_{50}$/mL in 15 μL DMEM or 5×10^7 $TCID_{50}$/mL in 15 μL DMEM) was injected into the intramedullary cavity ($N=6$ mice per treatment group). The quadriceps-patellar complex was then repositioned and the medial arthrotomy was repaired with 5-0 Vicryl suture. One week later, three mice of each group were sacrificed and femoral bone and marrow were isolated in TRIzol for gene expression analysis. Four weeks after injection, the remaining three mice were harvested for radiographic analysis via microcomputed tomography (microCT) (see again Supplementary Table S2 for animal allocation).

Real-time polymerase chain reaction

β-Catenin expression was analyzed in both human BMSC and murine bone tissue. qRT-PCR was performed 3 days postlentiviral transfection with human BMSCs or 1 week postlentiviral intramedullary injection with murine bone. Total RNA from cells for real-time polymerase chain reaction evaluation was extracted using TRIzol reagent (Invitrogen). Murine bone tissue was homogenized in 2 mL of TRIzol reagent per femur using mortar with liquid nitrogen. After homogenization, insoluble material from the homogenate was removed by centrifuging at 10,000 rpm for 10 min at 4°C. A total of $n=3$ replicates for both human and mice samples per treatment group were used for RNA studies. The following primer sequences were used for *β-catenin*, human: 5′-ATG GCTACTCAAGCTGAC-3′ and 5′-CAGCACTTTCAGCAC TCTGC-3′; mouse: β-catenin, forward primer 5′-gtgctatctgtc tgctctagta-3′, reverse primer 5′-cttcctgtttagttgcagcatc-3′.

Calvarial lentiviral injection

Our second mouse model assessed the effects of *β-catenin* knockdown in bone repair. In this study, subcutaneous injection of lentiviral encoding shRNA was performed overlying the calvaria followed by bone defect creation. After anesthesia, the skin overlying the calvaria was sterilized with Betadine scrub. Subcutaneous injection in the midline overlying the frontoparietal bones was performed using a sterile 30-gauge needle, either delivering phosphate-buffered saline (PBS) vehicle control (100 μL) or *β-catenin* shRNA or eGFP-shRNA control (7.8×10^6 $TCID_{50}$/mL in 100 μL DMEM or $7.8\times10^6\times10^7$ $TCID_{50}$/mL in 100 μL DMEM) ($N=3$–5 mice per treatment group, see again Supplementary Table S2 for animal allocation). One week postinjection, 1.8 mm bone defects were created in either the frontal or parietal bones for all lentivirus-treated mice. Before injury and 1 week postinjection, representative samples were examined for domains of GFP expression after viral injection. Next, and after anesthesia, the skin overlying the calvaria was shaved and aseptically prepared using Betadine scrub. The frontoparietal bones were exposed via a midline anterior to posterior incision. The overlying pericranium was gently removed from the right frontal bone and left parietal bones using a cotton swab. A 1.8 mm full-thickness right frontal bone defect and 1.8 mm full-thickness left parietal bone defect were created using a microsurgical drill with a 1.8-mm-diameter trephine burr. Meticulous care was taken to protect the neighboring sagittal, posterofrontal and coronal sutures, and the underlying dura mater. Calvarial defect sites were irrigated by saline. Finally, the skin was sutured and the animal was monitored as per established postoperative protocols.

microCT imaging and analyses

Femur samples were harvested 4 weeks postviral injection, and calvarial samples were harvested 4 weeks post-defect creation (see Supplementary Fig. S2 for a time line of animal studies). Samples were fixed in 4% paraformaldehyde for 24 h, transferred to PBS, and scanned using a high-resolution microCT (SkyScan 1294; Bruker microCT N.V) at an image resolution of 10 μm, with the following settings: 1 mm aluminum filter, X-ray voltage of 65 kVp, anode current of 153 μA, exposure time of 65 ms, frame averaging of 4, and rotation step of 0.3°. Three-dimensional (3D) images were then reconstructed from the two-dimensional (2D) X-ray projections by implementing the Feldkamp algorithm using a commercial software package NRecon software (2.0.4.0 SkyScan). For the 3D morphometric analyses of images, CTVox and CTAn software (1.13 SkyScan) were used.

For analysis of trabecular bone formation in femoral samples, regions of interest were drawn to select only metaphyseal intramedullary trabecular bone with a proximal to distal length of 1.225 mm (35 slices at 0.035 mm each). Trabecular bone formation was analyzed with a threshold value of 75 to all samples to isolate mineralized bone for bone volume (BV) and tissue volume (TV) measurements and calculations. Two-dimensional X-ray images were obtained by the creation of an axial cut through the center of the defect area. The bone mineral density (BMD) and BV density (BV/TV) were calculated from binary X-ray images.

For calvarial defect analysis, a cylindrical volume of interest centered around each defect site was defined as the 1.8 mm in diameter and 1 mm in height with a threshold value of 80. BV and TV measurements were calculated from analyses performed for a volume of 100 slices ($\sim$1 mm). The amount of bone formation was analyzed and quantified in three different ways. First, BV and BV density (BV/TV) were calculated from binary X-ray images. Second, bone fractional area (BFA) was calculated by using CTVox to create a 3D rendering of calvarial defect and measuring pixels of bone in defect divided by total defect area using Photoshop (Adobe, San Jose, CA). Finally, a bone healing score from 0 to 4 was assigned by three blinded observers according to previous published grading scales for calvarial defect healing.[20] Briefly, the grading system was as follows: 0—no bone formation, 1—few bony spicules dispersed through defect, 2—bony bridging only at defect borders,

3—bony bridging over partial length of defect, and 4—bony bridging the entire span of defect at longest point.

Histologic analysis

After radiographic imaging, samples were transferred to 14% ethylenediaminetetraaceticacid for decalcification for 14–21 days. Samples were then embedded in optimal cutting temperature compound and sectioned in a coronal plane at 10 μm thickness. To track potential lentiviral diffusion outside the injection site, histologic analysis was also performed on the following tissues at 4 and 8 weeks postinjection: femur, tibia, heart, lung, skin, subcutaneous adipose, stomach, small intestine, large intestine, kidney, liver, and spleen. Hematoxylin and eosin (H&E) staining was performed on serial sections.

Indirect immunofluorescent staining

For immunofluorescent staining, additional sections were incubated with the following primary antibodies: anti-GFP (A-21311, 1:200; Thermo Fisher Scientific), anti-Axin2 (ab32197, 1:200; Abcam Biotechnology), and anti-PCNA (ab18897, 1:200; Abcam). Sections were washed with PBS three times, 10 min each. Sections for PCNA staining were then permeabilized with 0.5% Triton X-100 for 15 min. All sections were blocked with 1% bovine serum albumin in PBS for 1 h at 25°C; antigen retrieval was by trypsin enzymatic antigen retrieval solution for 10 min at 37°C (ab970; Abcam). Axin-2, PCNA, and GFP primary antibodies were added to each section at their respective dilutions and incubated at 37°C for 1 h and then overnight at 4°C. Next, for Axin-2 and PCNA detection, a DyLight 594 goat anti-rabbit IgG (H + L) polyclonal (1:200) was used as the secondary antibody. Sections were counterstained with 4′,6-diamidino-2-phenylindole mounting medium (H-1500; Vector laboratories). All histological sections were examined under a Zeiss 700 confocal microscope (Zeiss, Thornwood, NY).

Statistical and power analyses

Means and standard deviations were calculated from numerical data, as presented in the text, figures, and figure legends. In figures, bar graphs represent means, whereas error bars represent one standard error. The means of groups were compared using the Mann–Whitney U test when only two data sets were being compared and by the Kruskal–Wallis test with *posthoc* tests of Bonferroni to compare more than two groups. Intraclass correlation coefficient was analyzed for independent scoring of defect sites. The statistical software SPSS for Windows Version 18.0 (SPSS) was used for all statistical analyses. Statistical significance was determined at the $p < 0.05$ level.

Two-sample sized analyses were performed to determine animal numbers for long bone intramedullary injection and calvarial studies. First, *in vitro* studies demonstrated large effect sizes >5. To obtain an estimate of effect sizes observable for pilot intramedullary studies, we examined the simplified scenario of control shRNA versus *β-catenin* shRNA at a single time point. For this scenario with six mice per group, a two-sample *t*-test will provide 80% power to detect effect sizes of at least two assuming a two-sided 0.05 level of significance.

Next, a second power analysis was performed for *in vivo* calvarial defect healing studies. Intramedullary injection studies demonstrated large effect sizes from 4.98. To obtain an estimate of the effect sizes observable for defect healing studies, we again examined the simplified scenario of control shRNA versus *β-catenin* shRNA at a single time point. For this scenario with three mice per group, a two-sample *t*-test will provide 80% power to detect effect sizes of at least 3.0 assuming a two-sided 0.05 level of significance.

Results

*Validation of lentiviral-encoded shRNA for β-*catenin *knockdown* in vitro *and* in vivo

In the first series of experiments, we aimed to validate the ability of this model to regulate the expression of *β-catenin.* First, we infected human BMSC with the lentivirus construct. As expected, qRT-PCR analysis demonstrated a significant knockdown of *β-catenin* expression, diminished by 73% compared with eGFP-shRNA control 1 week postinfection (Fig. 1A). We then sought to validate these results in an *in vivo* model using murine intramedullary femoral injection of lentivirus, adapted from our previous study.[19] In this study, intramedullary injection exposes the bone marrow milieu to lentiviral-delivered shRNA. Consistent with *in vitro* findings, after injection of lentivirus, there was a significant reduction in the expression of *β-catenin.* One week postinjection, animals were sacrificed and harvested murine bone and bone marrow demonstrated 52% decreased expression of *β-catenin* compared with control (Fig. 1B). The phenotypic consequences of intramedullary of *β-catenin* shRNA were next assessed. microCT reconstruction of murine femurs was performed at 4 weeks postinjection, and demonstrated a significant reduction in trabecular bone by all parameters examined. Using a colorized 3D reconstruction, trabecular bone of the distal femoral metaphysis and metadiaphysis was significantly reduced among the *β-catenin* shRNA group compared with the control shRNA (Fig. 1C). In addition, quantitative measurements of trabecular BMD were significantly diminished in the *β-catenin* shRNA group compared with control shRNA (Fig. 1D). A similar decrease was found in measurements of trabecular BV/TV in the *β-catenin* shRNA treatment group compared with control (Fig. 1E). In sum, lentiviral-delivered shRNA mediated knockdown of *β-catenin* both *in vitro* and *in vivo*, which in the case of intramedullary injections resulted in a significant trabecular bone phenotype.

*Lentiviral-delivered β-*catenin *shRNA significantly mediates frontal bone healing using microtomographic analysis*

We next sought to validate and examine lentiviral shRNA-mediated *β-catenin* knockdown in the context of bone repair. We first injected (i) PBS control, (ii) lentiviral control shRNA, or (iii) lentiviral *β-catenin* shRNA subcutaneously to locally infect the frontal and parietal calvarial bones. Validation of lentiviral delivery was confirmed by visualization of eGFP reporter activity at 1, 4, and 8 weeks postinjection within the frontal and parietal bones. At 1

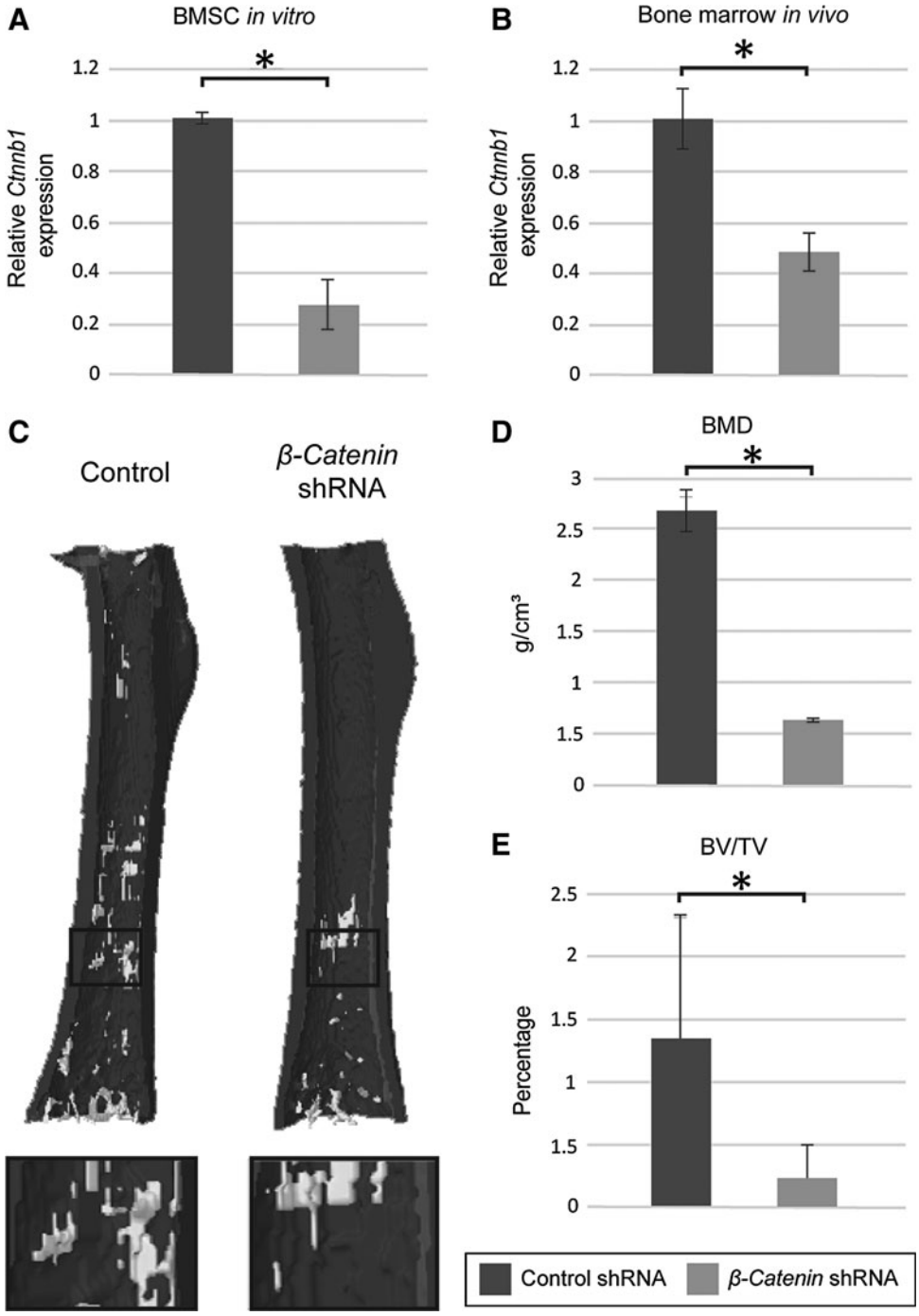

FIG. 1. Efficacy of lentiviral-delivered *β-catenin* shRNA *in vitro* and *in vivo*. **(A)** Human BMSCs were treated with lentivirus encoding *β-catenin* shRNA or control lentivirus-encoded enhanced GFP. Using qRT-PCR, a 73% knockdown was observed, $n = 3$ per group **(B–E)** Next, β-catenin shRNA lentivirus was applied *in vivo*, using a percutaneous intramarrow injection model, $n = 6$ per group. **(B)** After 1 week, 52% knockdown was observed by qRT-PCR. **(C)** After 4 weeks, microCT reconstructions showed a significant reduction in trabecular bone formation. **(D, E)** Trabecular BMD and BV/TV were significantly reduced with β-catenin shRNA treatment. $^*p < 0.01$ in comparison with control. shRNA, short hairpin; BMD, bone mineral density; BV, bone volume; TV, tissue volume; qRT-PCR, quantitative real time-polymerase chain reaction; BMSC, bone marrow mesenchymal stromal cell; GFP, green fluorescent protein; microCT, microcomputed tomography.

week, eGFP expression was observed in a strong and diffuse manner not only in the periosteum but also in dura mater and coronal suture mesenchyme. At 4 and 8 weeks post-subcutaneous injection, sustained periosteal and dural eGFP expression was observed, although a more patchy distribution was observed at the 8-week time point (Supplementary Fig. S3). In addition, a survey of eGFP reporter activity at distant sites by and large failed to identify eGFP expression (Supplementary Fig. S4). The only extracranial eGFP expression was observed within scattered stromal cells of the spleen, a finding consistent with prior reports.[21]

Next, we examined the phenotypic consequences on bone healing in mice that had undergone pretreatment with or without lentiviral shRNA-mediated *β-catenin* knockdown. Frontal or parietal bone defects (1.8 mm diameter) were created. Prior studies have documented that frontal bone defects undergo significant osseous repair overtime, while equal size defects in the parietal bone do not.[18,22] microCT reconstructions and analysis were performed at 4 weeks postoperative (Fig. 2). First, results confirmed the differential healing between frontal and parietal bone defects. Pronounced frontal bone defect healing was observed under control conditions (PBS control or control shRNA). In comparison, minimal bone healing was observed among parietal bone defects under control conditions. Next, the consequences of *β-catenin* knockdown were examined. In

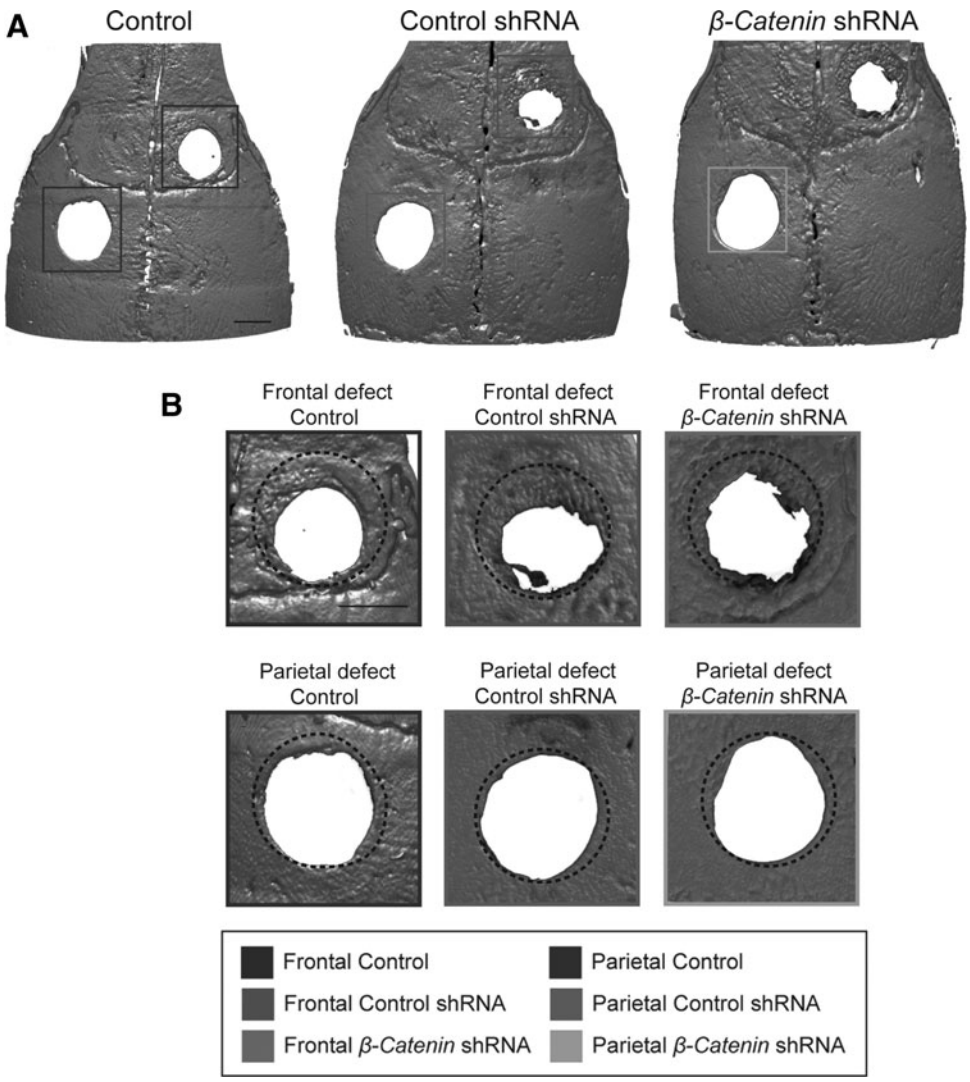

FIG. 2. Frontal bone healing is sensitive to lentivirus-delivered *β-catenin* shRNA. **(A)** microCT three-dimensional reconstruction images of frontal bone defects (*above*, *red*) and parietal bone defects (*below*, *blue*) were performed 4 weeks postoperatively. Animals were pretreated with PBS control, lentiviral-delivered control shRNA (random sequence shRNA with GFP), or lentiviral-delivered *β-catenin* shRNA with GFP. **(B)** High magnification of frontal and parietal defects. Original 1.8 mm defect size is outlined with a *dashed black circle*. Scale bars: 1 mm. PBS, phosphate-buffered saline.

those animals with *β-catenin* shRNA treatment, reduced frontal bone defect reossification was observed in comparison with PBS control or control shRNA. In contrast, parietal bone defect healing was minimally impacted among the *β-catenin* shRNA treatment group.

These differences were next confirmed by quantitative radiographic metrics (Fig. 3), including BV (Fig. 3A), percentage BV (BV/TV) (Fig. 3B), and BFA (Fig. 3C). Finally, after 3D-rendered models were generated, the extent of bone formation within the calvarial defect was scored using a bone healing score from 0 to 4 according to a previously published scale for calvarial healing[20] (Fig. 3D). Results confirmed that across all frontal bone defect groups and all quantitative metrics, significant reossification was observed in comparison with parietal bone defects. Control shRNA showed no difference to PBS control across any parameter. Across all quantitative endpoints, a significant reduction of frontal bone defect healing was noted with *β-catenin* shRNA treatment. In contrast, parietal bone defect healing was minimal under all conditions, and was predominantly unchanged among *β-catenin* shRNA-treated mice. These results confirmed prior observations regarding the greater healing capacity of frontal bone defects, and suggested that normal frontal bone healing required intact Wnt/β-catenin signaling.

Lentiviral-delivered β-catenin shRNA inhibits frontal bone osteogenesis

To further define effects of *β-catenin* knockdown, histologic analyses of frontal and parietal bone defects were next performed. H&E-stained histologic sections confirmed microCT findings (Fig. 4). Control-treated frontal bone defects demonstrated extensive new woven bone either contiguous with the bone defect margins or seen as small detached trabeculae within the defect midsubstance (Fig. 4A). In contrast, frontal bone defect healing was significantly reduced with lentiviral-delivered *β-catenin* shRNA, with reduced new bone formation at the defect edge and predominantly undifferentiated mesenchyme within the defect midsubstance (Fig. 4B). Consistent with radiographic findings, control shRNA-treated parietal bone defects were sharply marginated at the defect edge, with little new bone formation (Fig. 4C). A similar histologic appearance of parietal bone defects was observed among the *β-catenin* shRNA-treated groups (Fig. 4D). Histologic results were confirmed by histomorphometric means, either by measuring bone area per high-power field within the defect site (Fig. 4E) or relative remaining bone defect length (Fig. 4F).

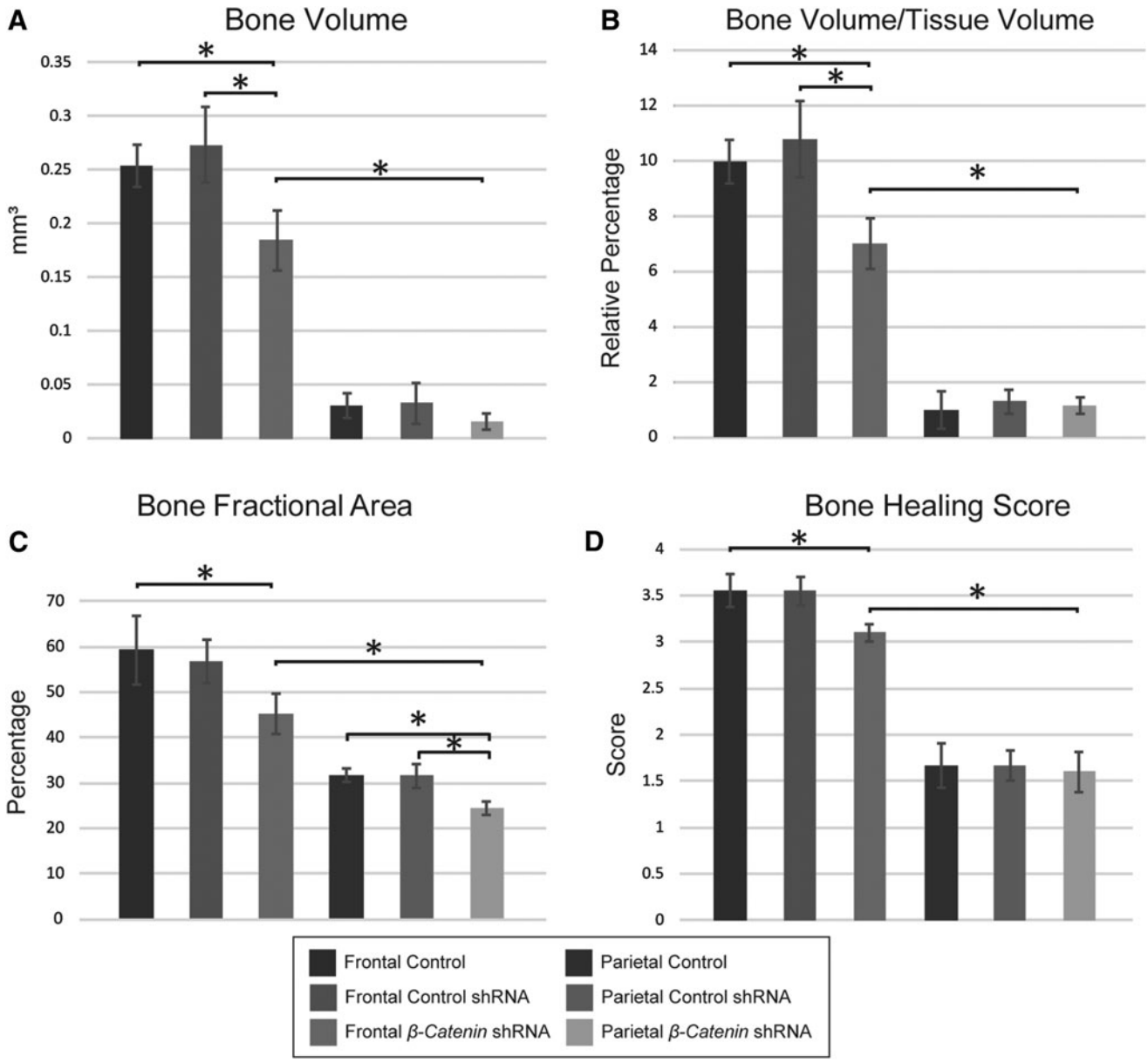

FIG. 3. microCT quantification of calvarial defect healing. microCT quantitative analysis performed at 4 weeks post-operatively. Animals were pretreated with PBS control, lentiviral-delivered control shRNA (random sequence shRNA with GFP), or lentiviral-delivered *β-catenin* shRNA with GFP. Frontal bone defects are shown in *red*, while parietal bone defects are shown in *blue*. **(A)** BV, **(B)** BV/TV, **(C)** bone fractional area, and **(D)** semiquantitative healing score (grade) after 4 weeks. A significant reduction among frontal defect healing was noted across all markers with *β-catenin* shRNA treatment. $N=3$ mice per PBS and shRNA control group; $N=5$ mice per *β-catenin* shRNA group. $^*p<0.05$.

Next, more detailed immunohistochemical analysis of frontal and parietal bone defects was examined under control shRNA or *β-catenin* shRNA treatment conditions (Fig. 5). To assess the functional changes to Wnt/β-catenin signaling, the transcriptional target Axin-2 was assessed[23] (Fig. 5A). Under control shRNA conditions, Axin-2 expression as detected by immunofluorescent staining was most clearly observed at the leading bone defect edge and was most prominent within frontal bone defects (see white arrowheads, Fig. 5A). A significant decrease in Axin-2 expression was observed among the *β-catenin* shRNA treatment groups. This reduction in Axin-2 immunofluorescent staining was most prominent among frontal bone defects. A less dramatic reduction in Axin-2 immunostaining was also observed among *β-catenin* shRNA-treated parietal bone defects. Finally, immunofluorescent staining for PCNA was performed as a well-established marker of cell proliferation.[24] Predominantly, nuclear staining was observed across all sections with weak cytoplasmic immunostaining. Similar to the domain of Axin-2 expression, strong PCNA expression was predominantly localized to the leading reossification front of the frontal or parietal bones. A marked decrease in PCNA immunostaining was observed among the *β-catenin* shRNA-treated defects, which was again most notable within the frontal bone defects.

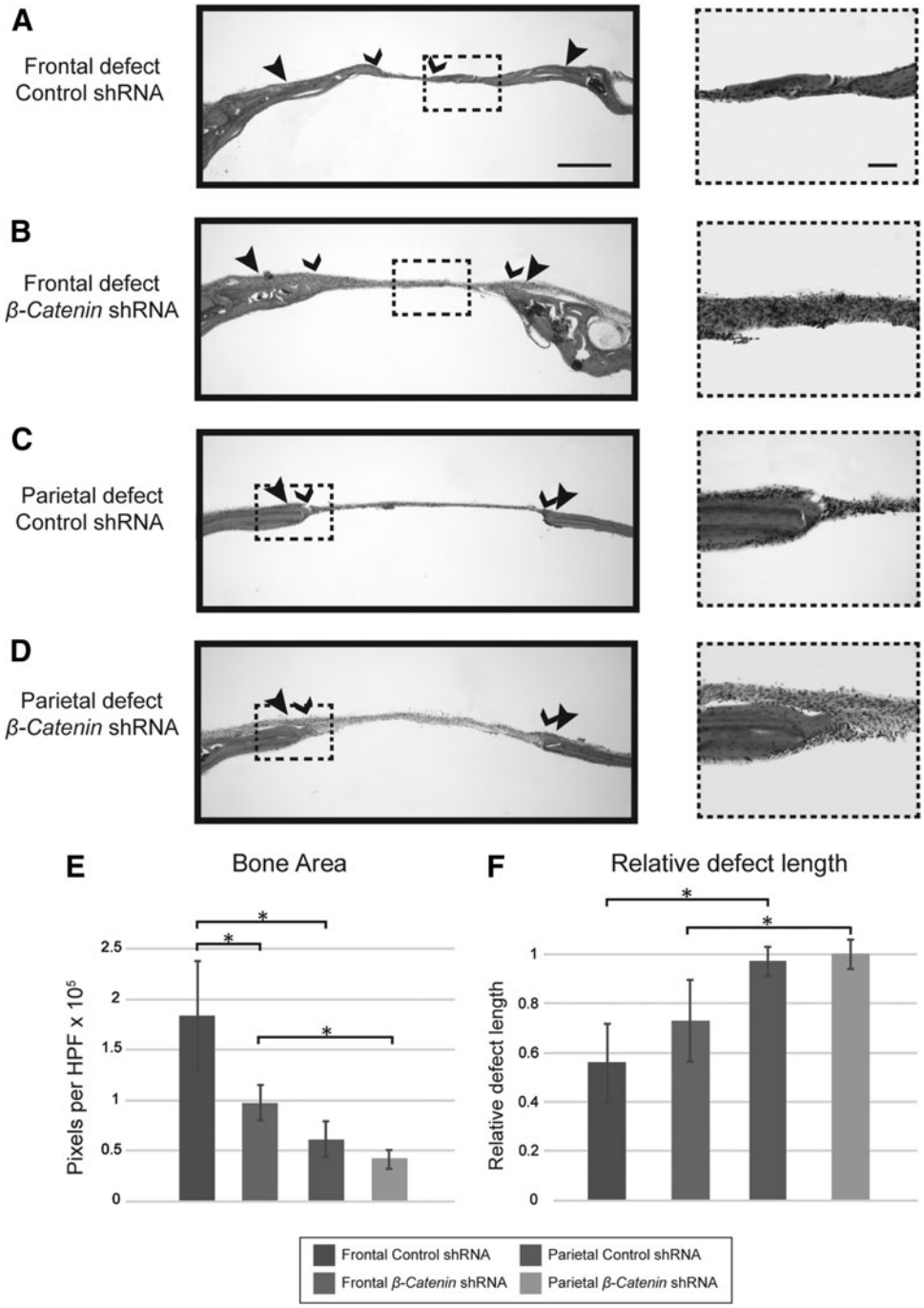

FIG. 4. Histologic examination of frontal and parietal bone defect healing with *β-catenin* shRNA. **(A–D)** Coronal cross-sectional images of bone defects at low-magnification (4×) and corresponding (10×) images. **(A)** Frontal bone defects with lentiviral-delivered control shRNA. **(B)** Frontal bone defects with lentiviral-delivered *β-catenin* shRNA. **(C)** Parietal bone defects with lentiviral-delivered control shRNA. **(D)** Parietal bone defects with lentiviral-delivered *β-catenin* shRNA. **(E, F)** Histomorphometric analysis of serial hematoxylin and eosin sections, quantifying **(E)** bone area, and **(F)** residual, relative bone defect length. $*p < 0.05$; $N = 3$ mice per PBS and shRNA control group; $N = 5$ mice per *β-catenin* shRNA group: $N = 12$ images analyzed per sample. Large arrowheads indicate original defect location, while small arrowheads indicate extent of bone healing. Scale bars: 200 μm for 4× images and 100 μm for 10× images.

Discussion

The canonical Wnt/β-catenin pathway has long been studied as an intrinsic mechanism for bone development and regeneration. Although there are many available *in vivo* models for knockdown of this pathway, including conditional knockout and siRNA inhibition,[10–12] none offers a targeted, stable, and prolonged avenue for *β-catenin* knockdown. In this study, we used a lentiviral-delivered shRNA vector targeted to *β-catenin*. Our results resulted in significant bone morphologic changes in both an intramedullary injection model in the long bone and a bone defect model.

Wnt signaling is known as an important regulatory pathway for bone formation by inducing osteogenic differentiation and inactivating pathways for osteopenic states. In mesenchymal stem cells, *β-catenin* has been shown to promote differentiation into osteoblasts and suppress differentiation into adipogenic or chondrogenic lineages by upregulation of osteogenic regulators such as Runx2, Dlx5, and Osterix.[25] Downstream mediators of *β-catenin* likely lead to normal osteogenic development by potentiating growth of osteoblasts; however, studies have found disturbances in *β-catenin* to also regulate osteoclast differentiation.[26,27] Conditional *β-catenin* knockout mice demonstrated a dramatic increase in osteoclast

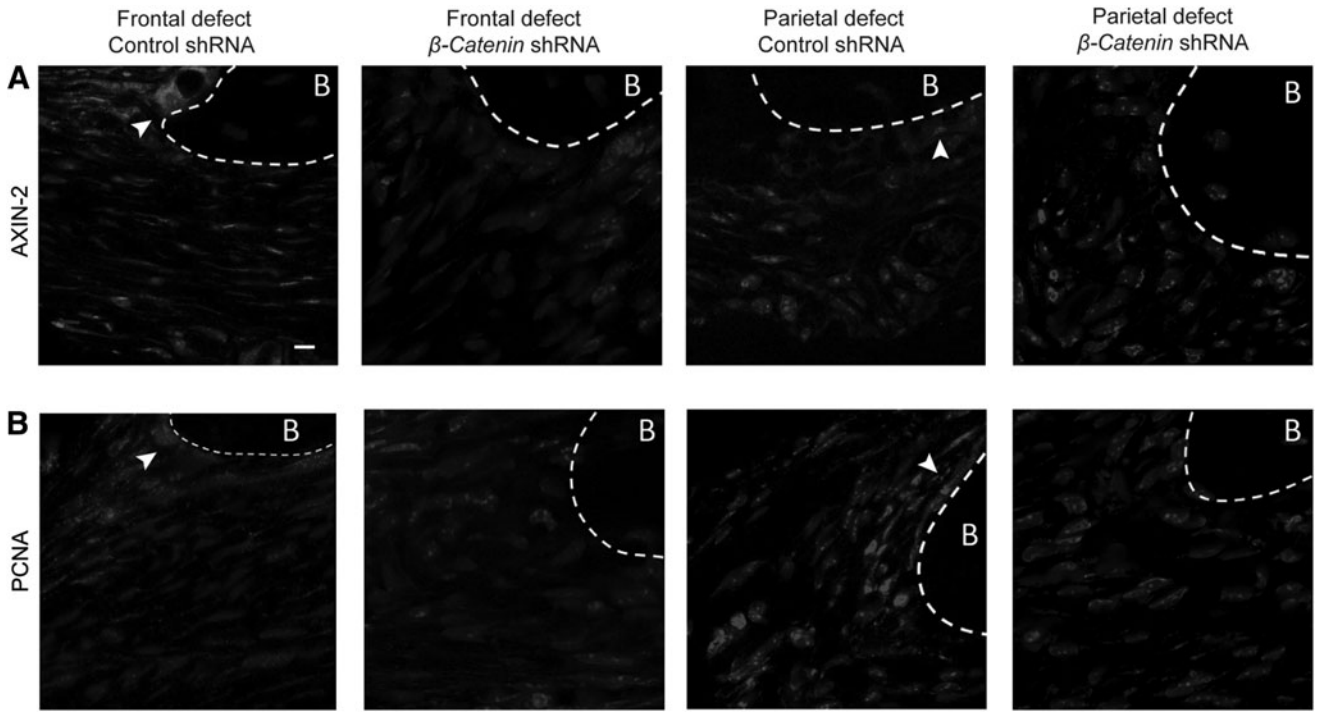

FIG. 5. Immunohistochemical examination of frontal and parietal bone defect healing with *β-catenin* shRNA. Immunofluorescent staining performed on sections of frontal and parietal bone defects at 4 weeks postoperative among control shRNA and *β-catenin* shRNA treatment conditions. **(A)** High-magnification (40×) images of Axin-2 immunofluorescent staining at the bone defect edge, appearing *red*. **(B)** High-magnification (40×) images of proliferating cell nuclear antigen immunofluorescent staining at the defect edge, appearing *red*. Cells were counterstained with 4′,6-diamidino-2-phenylindole (*blue*). *White arrow heads* point to immunofluorescent staining at the leading reossification front, while *dashed white lines* indicate the bone (B) margin. Scale bar: 10 μm.

numbers,[27] indicating the multiple roles *β-catenin* plays in bone homeostasis. Although cell proliferation and apoptosis are well-known methods in which *β-catenin* regulates bone development, its function in multiple downstream regulator domains means further study is required to fully understand the effects of *β-catenin* knockdown on osteoprogenitor cells and bone formation.

As the Wnt/*β-catenin* pathway functions in both bone maintenance and repair, we wanted to validate this method of *β-catenin* knockdown in a bone healing model. Initial studies have determined differential healing pathways in calvarial bones due to embryological differences in frontal and parietal bone development. As the frontal bone is derived from a neural crest origin, it has been shown to demonstrate enhanced bone healing along with increased Wnt/*β-catenin* pathway activation.[18] Our results have confirmed previous reports by Li *et al.* that frontal bone healing is enhanced due to the Wnt/*β-catenin* pathway,[22] and we have further demonstrated that knockout of this pathway confers diminished frontal bone healing as well as dramatically decreased expression of downstream targeted genes, including Axin-2.

Interestingly, despite our knockdown of the *β-catenin* pathway, frontal bone healing was still more significant than parietal bone healing. This was found in both the control and *β-catenin* shRNA groups, indicating that knockout of the Wnt/*β-catenin* pathway does not fully diminish the differential pathways of bone healing. This is likely due to differences in embryological origin of frontal and parietal bones, resulting in other pathways known to play important roles in calvarial osteogenesis, including transforming growth factor-β, bone morphogenetic protein, and fibroblast growth factor (FGF).[28] For example, Quarto *et al.* have found differential expression of FGF receptors between neural crest-derived and parietal mesoderm-derived osteoblasts,[29,30] suggesting intrinsic differences in frontal and parietal bone healing. Congruent with these observations, our data suggest that Wnt signaling interacts with multiple pathways that govern the enhanced osteogenic potential in frontal bone healing. In the future, it will be crucial to define the interplay between these signaling pathways in the frontal bone, which our model of localized *β-catenin* knockdown may facilitate. In addition, by specifically knocking down *β-catenin,* we will be better able to tease out the regulatory relationship between the Wnt pathway and osteoinductive ligands.

In summary, we have generated a novel model for studying the stable and localized inhibition of the Wnt/β-catenin pathway through a lentiviral vector both in *in vitro* and *in vivo* applications. Lentiviral-delivered *β-catenin* shRNA model allows for specific and localized Wnt/*β-catenin* signaling blockade and can be used for further investigation of the importance of locoregional Wnt/β-catenin signaling in bone regeneration. Validation of this model both in static and dynamic *in vivo* models demonstrates the breadth of Wnt/β-catenin inhibition on both bone maintenance and regeneration.

Acknowledgments

The authors thank Dr. Greg Asatrian for his excellent technical assistance. The present work was supported by the NIH/NIAMS (R01 AR070773, K08 AR068316), Department of Defense (PR170080, PR170115, BA160256), American Cancer Society (Research Scholar Grant, RSG-18-027-01-CSM), the Orthopaedic Research and Education Foundation with funding provided by the Maryland Stem Cell Research Foundation, and the Musculoskeletal Transplant Foundation. The content is solely the responsibility of the authors and does not necessarily represent the official views of the National Institute of Health. They thank the JHU microscopy facility (S10OD016374, S10OD016374) for the technical assistance.

Authors' Contributions

L.Z.: collection and/or assembly of data, article writing; L.C.: collection and/or assembly of data, article writing; J.X.: collection and/or assembly of data; C.A.M.: collection and/or assembly of data; N.Y.: collection and/or assembly of data; E.Z.: collection and/or assembly of data; K.T.: provision of study material, financial support; C.S.: provision of study material, financial support; S.P.: provision of study material; A.W.J.: provision of study material, financial support, and final approval of article.

Disclosure Statement

No competing financial interests exist.

References

1. MacDonald, B.T., Tamai, K., and He, X. Wnt/beta-catenin signaling: components, mechanisms, and diseases. Dev Cell **17,** 9, 2009.
2. Krishnan, V., Bryant, H.U., and Macdougald, O.A. Regulation of bone mass by Wnt signaling. J Clin Invest **116,** 1202, 2006.
3. Liu, F., Kohlmeier, S., and Wang, C.Y. Wnt signaling and skeletal development. Cell Signal **20,** 999, 2008.
4. James, A.W., Shen, J., Zhang, X., *et al.* NELL-1 in the treatment of osteoporotic bone loss. Nat Commun **6,** 7362, 2015.
5. Nishiya, N., Oku, Y., Kumagai, Y., *et al.* A zebrafish chemical suppressor screening identifies small molecule inhibitors of the Wnt/β-catenin pathway. Chem Biol **21,** 530, 2014.
6. Jin, H., Wang, B., Li, J., *et al.* Anti-DKK1 antibody promotes bone fracture healing through activation of beta-catenin signaling. Bone **71,** 63, 2015.
7. Huelsken, J., Vogel, R., Erdmann, B., Cotsarelis, G., and Birchmeier, W. Beta-catenin controls hair follicle morphogenesis and stem cell differentiation in the skin. Cell **105,** 533, 2001.
8. Tan, X., Behari, J., Cieply, B., Michalopoulos, G.K., and Monga, S.P. Conditional deletion of beta-catenin reveals its role in liver growth and regeneration. Gastroenterology **131,** 1561, 2006.
9. Singh, Y., Port, J., Schwarz, M., and Braeuning, A. Genetic ablation of beta-catenin inhibits the proliferative phenotype of mouse liver adenomas. Br J Cancer **111,** 132, 2014.
10. Zhang, X.F., Tan, X., Zeng, G., *et al.* Conditional beta-catenin loss in mice promotes chemical hepatocarcinogenesis: role of oxidative stress and platelet-derived growth factor receptor alpha/phosphoinositide 3-kinase signaling. Hepatology **52,** 954, 2010.
11. Dudek, H., Wong, D.H., Arvan, R., *et al.* Knockdown of β-catenin with dicer-substrate siRNAs reduces liver tumor burden in vivo. Mol Ther **22,** 92, 2014.
12. Wang, Z., and Chen, Q. β-Catenin knockdown inhibits the proliferation of human glioma cells in vitro and in vivo. Exp Ther Med **11,** 1059, 2016.
13. Jackson, A.L., and Linsley, P.S. Recognizing and avoiding siRNA off-target effects for target identification and therapeutic application. Nat Rev Drug Discov **9,** 57, 2010.
14. Dahlman, J.E., Barnes, C., Khan, O., *et al.* In vivo endothelial siRNA delivery using polymeric nanoparticles with low molecular weight. Nat Nanotechnol **9,** 648, 2014.
15. Oliveira, S., Storm, G., and Schiffelers, R.M. Targeted delivery of siRNA. J Biomed Biotechnol **2006,** 63675, 2006.
16. Sakuma, T., Barry, M.A., and Ikeda, Y. Lentiviral vectors: basic to translational. Biochem J **443,** 603, 2012.
17. Vlachaki, M.T., Hernandez-Garcia, A., Ittmann, M., *et al.* Impact of preimmunization on adenoviral vector expression and toxicity in a subcutaneous mouse cancer model. Mol Ther **6,** 342, 2002.
18. Quarto, N., Wan, D.C., Kwan, M.D., Panetta, N.J., Li, S., and Longaker, M.T. Origin matters: differences in embryonic tissue origin and Wnt signaling determine the osteogenic potential and healing capacity of frontal and parietal calvarial bones. J Bone Miner Res **25,** 1680, 2010.
19. James, A.W., Shen, J., Khadarian, K., *et al.* Lentiviral delivery of PPARgamma shRNA alters the balance of osteogenesis and adipogenesis, improving bone microarchitecture. Tissue Eng A **20,** 2699, 2014.
20. Spicer, P.P., Kretlow, J.D., Young, S., Jansen, J.A., Kasper, F.K., and Mikos, A.G. Evaluation of bone regeneration using the rat critical size calvarial defect. Nat Protoc **7,** 1918, 2012.
21. Brown, B.D., Sitia, G., Annoni, A., *et al.* In vivo administration of lentiviral vectors triggers a type I interferon response that restricts hepatocyte gene transfer and promotes vector clearance. Blood **109,** 2797, 2007.
22. Li, S., Quarto, N., Senarath-Yapa, K., Grey, N., Bai, X., and Longaker, M.T. Enhanced activation of canonical Wnt signaling confers mesoderm-derived parietal bone with similar osteogenic and skeletal healing capacity to neural crest-derived frontal bone. PLoS One **10,** e0138059, 2015.
23. Jho, E.H., Zhang, T., Domon, C., Joo, C.K., Freund, J.N., and Costantini, F. Wnt/beta-catenin/Tcf signaling induces the transcription of Axin2, a negative regulator of the signaling pathway. Mol Cell Biol **22,** 1172, 2002.
24. Muskhelishvili, L., Latendresse, J.R., Kodell, R.L., and Henderson, E.B. Evaluation of cell proliferation in rat tissues with BrdU, PCNA, Ki-67(MIB-5) immunohistochemistry and in situ hybridization for histone mRNA. J Histochem Cytochem **51,** 1681, 2003.
25. Kang, S., Bennett, C.N., Gerin, I., Rapp, L.A., Hankenson, K.D., and Macdougald, O.A. Wnt signaling stimulates osteoblastogenesis of mesenchymal precursors by suppressing CCAAT/enhancer-binding protein alpha and peroxisome

proliferator-activated receptor gamma. J Biol Chem **282,** 14515, 2007.
26. Day, T.F., Guo, X., Garrett-Beal, L., and Yang, Y. Wnt/beta-catenin signaling in mesenchymal progenitors controls osteoblast and chondrocyte differentiation during vertebrate skeletogenesis. Dev Cell **8,** 739, 2005.
27. Holmen, S.L., Zylstra, C.R., Mukherjee, A., *et al.* Essential role of beta-catenin in postnatal bone acquisition. J Biol Chem **280,** 21162, 2005.
28. Li, S., Meyer, N.P., Quarto, N., and Longaker, M.T. Integration of multiple signaling regulates through apoptosis the differential osteogenic potential of neural crest-derived and mesoderm-derived osteoblasts. PLoS One **8,** e58610, 2013.
29. Quarto, N., Behr, B., Li, S., and Longaker, M.T. Differential FGF ligands and FGF receptors expression pattern in frontal and parietal calvarial bones. Cells Tissues Organs **190,** 158, 2009.
30. Li, S., Quarto, N., and Longaker, M.T. Activation of FGF signaling mediates proliferative and osteogenic differences between neural crest derived frontal and mesoderm parietal derived bone. PLoS One **5,** e14033, 2010.

Address correspondence to:
Aaron W. James, MD, PhD
Department of Pathology
Johns Hopkins University
Ross Research Building, Room 524A
720 Rutland Avenue
Baltimore, MD 21205

E-mail: awjames@jhmi.edu

Received: November 6, 2017
Accepted: May 24, 2018
Online Publication Date: August 17, 2018